Ghandour *Swiss J Geosci* (2020) 113:3
https://doi.org/10.1186/s00015-020-00357-3

SGG SGS sc | nat
Swiss Journal of Geosciences

ORIGINAL PAPER Open Access

Paleoenvironmental changes across the Paleocene–Eocene boundary in West Central Sinai, Egypt: geochemical proxies

Ibrahim Mohamed Ghandour[1,2*]

Abstract

A geochemical analysis has been conducted on twenty-six sediment samples spanning the P–E boundary interval collected from the Esna Shale in three well-dated stratigraphic sections in west-central Sinai, Egypt to interpret paleoenvironmental changes associated with the P–E boundary events. The Esna Shale consists of hemipelagic marine shales and marls and it is subdivided stratigraphically into the uppermost Paleocene Hanadi Member unconformably overlain by the lowermost Eocene Dababiya Quarry Bed (DQB) and El-Mahmiya members. A variety of geochemical proxies including the Al-normalized elemental concentrations and redox-related elemental ratios and parameter (V/Cr, V/V + Ni and Mn*) and productivity indicators (P_{org} and Ba_{bio}) were employed for paleoceanographic interpretations. Across the P–E transition, the concentrations of SiO_2, TiO_2, Al_2O_3 Fe_2O_3, MgO, V, Cr, Ni, Cu, Rb, and Zr notably increased, whereas the concentrations of CaO, MnO, Sr, and Zn abruptly decreased. The variation in the elemental concentrations is attributed to the carbonate dissolution because of increased ocean acidification as well as a brief increase in the detrital influx associated with the brief humid interval at the base of the Eocene. The Al-normalized detrital-related elements (Ti, Zr, and Rb) values show a relatively homogeneous profile suggesting a uniform detrital input from an unchanged source rock. The simultaneous significant increase in the V/Cr and V/V + Ni ratios and enrichment of Ni, Cu, and Zn in the sediments of the DQB suggest that the depositional basin experienced dysoxic to slightly anoxic bottom conditions. The coeval increase in the P_{org} and Ba_{bio} in the sediments of the DQB suggests an increase in nutrients availability and consequently primary productivity possibly due to enhanced upwelling during early Eocene.

Keywords: P–E boundary, West-central Sinai, Tethyan margin, Paleoceanography, Paleoredox, Paleoproductivity

1 Introduction

The Paleocene–Eocene boundary (P–E) interval (56 Ma ago) known as the Paleocene–Eocene thermal maximum (PETM; Kennett and Stott 1991) is a significant and short-lived (170 to ~ 217 kyr; Röhl et al. 2007; Murphy et al. 2010) extreme and abrupt global warming event marked by an abrupt increase in the sea surface and deep-sea temperatures by 5–8 °C and 6 °C, respectively (Sluijs et al. 2006; Zachos et al. 2006). This event had a profound impact on the atmospheric and oceanic circulation patterns and marine and terrestrial ecosystem. The sedimentary records across the PETM bear several lithological, mineralogical, geochemical and biological criteria explaining the environmental perturbations and ecosystem readjustments associated with this dramatic climatic warming (Gawenda et al. 1999). The most prominent criteria of this extreme global event are: (1) a remarkable negative (− 2 to − 7‰) carbon isotope excursion (CIE; Kennett and Stott 1991; Kender et al. 2012), (2) a rise of water salinity, (3) a drop of pH and dissolved oxygen and

Editorial handling: W. Winkler.

*Correspondence: ighandour@kau.edu.sa
[1] Marine Geology Department, Faculty of Marine Science, King Abdulaziz University, P.O. Box 80200, Jeddah 21589, Saudi Arabia
Full list of author information is available at the end of the article

shoaling of the CCD (Sluijs et al. 2007; Zachos et al. 2008; Westerhold et al. 2011; Keller et al. 2018), (4) extinction of 35–50% of deep-sea benthic foraminifera (Alegret et al. 2009), (5) turnover of planktonic foraminifera and calcareous nannofossils (Aubry et al. 2007; Self-Trail et al. 2012; Cao et al. 2018) and (6) diversification and migration of terrestrial mammals (Bowen et al. 2002). In addition, the high abundance of kaolinite and abrupt increase in eutrophic dinoflagellates in many shallow marine sedimentary sections spanning the PETM (Bolle and Adatte 2001, Crouch et al. 2003) suggest increased precipitation and runoff and enhanced marine productivity. The mechanism(s) and consequences of the PETM global changes has been a focus in several research efforts since its discovery.

Several terrestrial and marine sedimentary records spanning the PETM with characteristic carbon isotope excursion (CIE) and distinctive lithologic and biotic features have been documented at several localities worldwide (Speijer and Wagner 2002; McInerney and Wing 2011; Pälike et al. 2014; Schoon et al. 2015; Cao et al. 2018). Among of them, the Tethys is still the key region for investigating the mechanism of P–E global change (Gawenda et al. 1999; Soliman et al. 2011; Khozyem et al. 2013, 2015; Stassen et al. 2012; Gavrilova et al. 2018). The most extensive and continuous sedimentary record across the P–E boundary is documented from the southern margin of the Tethys. This record is known in Egypt as the Dababiya Quarry Beds (DQB) that was first described from the Dababiya, Luxor. In 2003, the DQB was selected as the Global Boundary Stratotype Section and Point (GSSP) for the basal Eocene (Dupuis et al. 2003). The DQB display distinctive lithological, biological, mineralogical and chemical attributes. With little variations from the type section, the DQB is recognized from the Paleogene sections in west-central Sinai (Khozyem et al. 2013; Faris et al. 2015; Obaidalla et al. 2017). Studies carried out in west-central Sinai concerned mainly with foraminiferal (Obaidalla et al. 2017) and calcareous nannoplankton (Abu Shama and Faris 2007; Faris et al. 2015) biostratigraphy. Paleoenvironmental, mineralogical and geochemical studies on the PETM in west-central Sinai are relatively rare (Bolle et al. 2000; Speijer and Wagner 2002; Khozyem et al. 2013).

The present study utilizes inorganic chemical composition of the P–E sedimentary record in west-central Sinai, Egypt to (1) reconstruct paleoenvironmental changes associated with the P–E boundary global perturbations in southern Tethys, (2) interpret elemental enrichments in terms of environmental response to the P–E boundary global events and (3) correlate the findings with the previous investigations in other Tethyan margin sections.

2 Geological background

At the end of the Paleocene, the Tethyan Ocean was an extensive northward deepening epicontinental basin covering most of Egypt, Israel, and Jordan. The southern margin of the Tethys was located in the northern tropical zone that was strongly affected by intermittent upwelling episodes (Speijer and Wagner 2002; Schulte et al. 2011). Many well preserved and widely distributed stratigraphic sections in North Africa and Arabian Craton contain biotic and geochemical evidence related with these upwelling episodes (Almogi-Labin et al. 1993). These sections display similar and distinctive features revealing the P–E major global changes. The most extensive and continuous P–E sedimentary records of distinctive lithologic, biotic and chemical characteristics at the southern margin of the Tethyan seaway are widely distributed in Egypt. In west-central Sinai, these strata are represented by continuous succession of hemipelagic sediments containing abundant and diverse microfossil assemblages (Bolle et al. 2000; Speijer and Wagner 2002; Khozyem et al. 2013; Faris et al. 2015; Obaidalla et al. 2017).

In west-central Sinai, the P–E upper bathyal (500–600 m water depth) grey to dark grey shales belonging to the lower Paleogene Esna Shale are well exposed at Wadi (W.) Matulla, W. Feiran and Gebel (G.) Mekattub (Fig. 1). The stratigraphy of these deposits is well constrained subdividing the Esna Shale into three members; the uppermost Paleocene Hanadi and the lowermost Eocene Dababiya Quarry Bed (DQB) and El-Mahmiya. The sediments of the Hanadi Member are dominated by light brown to light grey massive mudstones, varying in thickness laterally from 1.8 to 6 m because of syn-depositional faulting (Faris et al. 2015). The Dababiya Quarry Bed (DQB) Member is a sharp-based distinctive horizon varying in thickness from 0.5 to 0.9 m. It consists at the base of dark grey massive shales (3–12 cm thick) sharply overlain by light to medium grey silty mudstone (~ 25 cm thick) with abundant coprolites, phosphate nodules and fish remains. The last bed contains *Chondrites* trace fossils (Faris et al. 2015). The upper part of the DQB consists of marl bed up to 40 cm thick. The P–E boundary is placed at the base of a dark grey shales that define the contact between the Hanadi and Dababiya Quarry members (Bolle et al. 2000; Speijer and Wagner 2002; Khozyem et al. 2013). The dark grey clay layer is known at W. Nukhul section by Khozyem et al. (2013) as condensed clay-rich interval. The base of dark grey shales correlates with the base of the carbon isotope excursion (CIE) level. This level is consistent with the base of the Eocene Series in the Dababiya (GSSP) in Egypt (Dupuis et al. 2003; Aubry et al. 2007). Calcareous nannofossil biostratigraphy (Faris et al. 2015) suggests a short hiatus (absence of the NP9b subzone) at the P–E boundary.

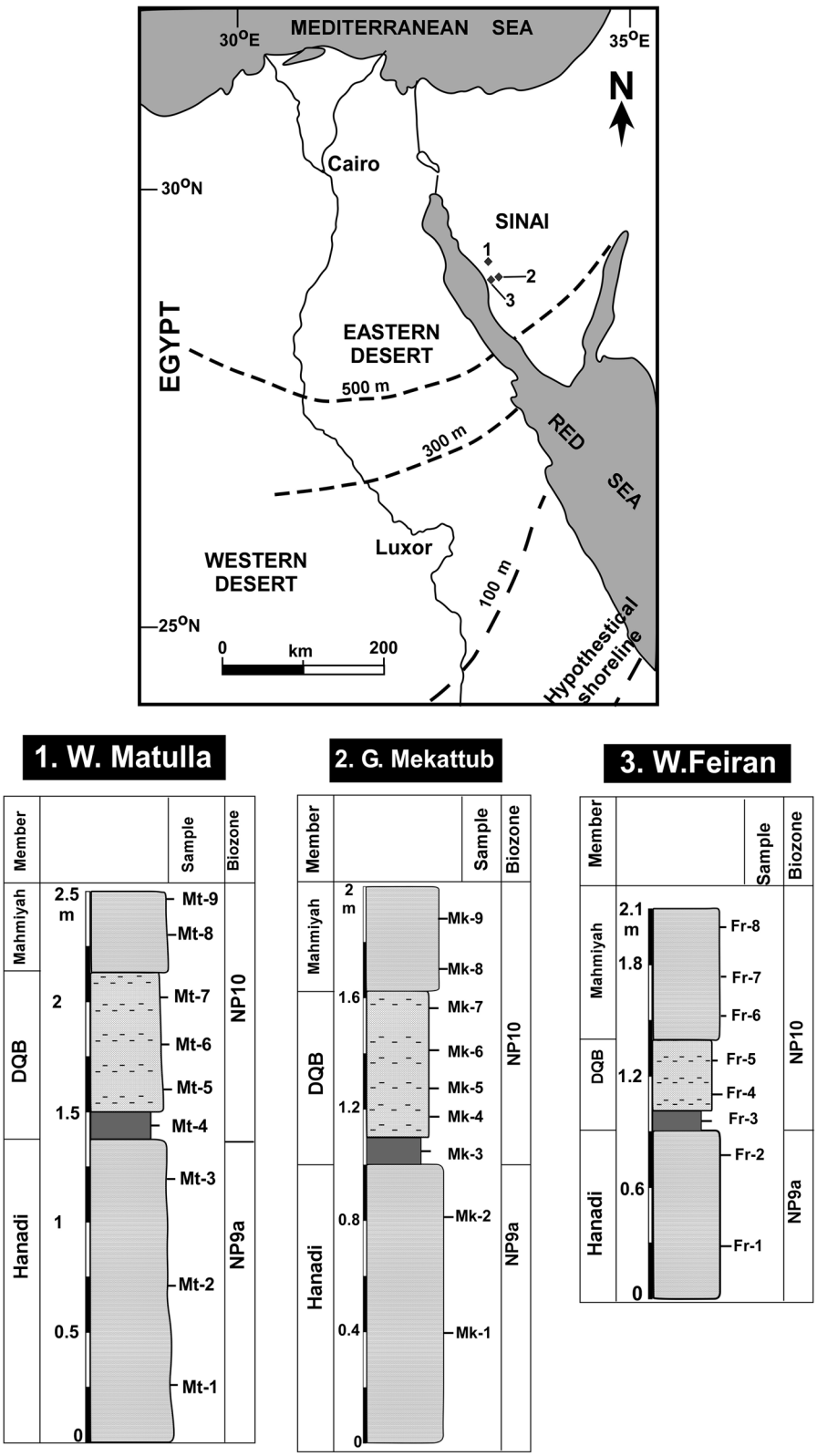

Fig. 1 Location map of the study area showing the locations of the stratigraphic sections. The stratigraphic sections and the biostratigraphic zonation are modified after Faris et al. (2015)

The DQB rests unconformably over the latest Paleocene Hanadi Member with no evidence for subaerial exposure (Schulte et al. 2011). The sediments of the Hanadi Member were deposited during the late Eocene sea-level high stand (HST), whereas the sediments of the DQB were deposited during the early Eocene rapid sea-level rise (TST) with poorly preserved lowstand deposits (Speijer and Wagner 2002).

The paleoclimate of the P–E boundary interval in west-central Sinai was interpreted relying on clay minerals analysis (Bolle et al. 2000; Khozyem et al. 2013). The enrichment of palygorskite, sepiolite, and illite in the sediments of pre-PETM at W. Nukhul west-central Sinai (Khozyem et al. 2013) suggests a dominantly arid climate, whereas the abrupt increase of the kaolinite content in the lowermost sediments of the PETM indicates a short period of warm humid conditions. The increase in the smectite content in the lower Eocene sediments suggests dominantly arid climate punctuated by short intensive humid intervals (Khozyem et al. 2013).

3 Materials and methods

Twenty-six fresh rock samples spanning the P–E boundary interval were collected from W. Matulla (9 samples), G. Mekattub (9 samples) and W. Feiran (8 samples) west-central Sinai (Fig. 1). Conventional XRF technique was conducted at the Department of Geosciences, Osaka City University, Japan to determine the chemical composition of the sediments. Glass beads were prepared by fusing 1.8 g of dry powdered sample with 3.6 g of spectroflux ($Li_2B_4O_7$ 20%, $LiBO_2$ 80%), 0.54 g of oxidant $LiNO_3$, traces of LiI and 4.2 g of $Li_2B_4O_7$ at 800 °C for 120 s and 1200 °C for 200 s (Tawfik et al. 2017). The analysis was carried out using a RIGAKU RIX 2100 X-ray fluorescence spectrometer (XRF), equipped with Rh/W dual-anode X-ray tube under 50 kV and 50 mA accelerating voltage and tube current, respectively. The accuracy of the analyses was estimated to be ± 2–3% for major elements and ± 10–15% for trace elements. Precision was measured at < 0.5% for major elements and < 7% for trace elements. Total iron is introduced as $Fe_2O_3^t$ and major and trace elements are reported as wt% and μg/g, respectively. Trace-element concentrations are normalized to Al to correct dilution by organic matter and authigenic minerals, to compensate the effect of mineralogy and grain size on elemental contents and to differentiate the detrital, biogenic and authigenic origin of the elements (e.g., Riquier et al. 2006; Soua et al. 2011; Khozyem et al. 2015). The enrichment factor (EF) of the environmentally significant elements is determined (Algeo and Maynard 2004; Rimmer 2004) by normalizing the element against the average shale composition (Li and Schoonmaker 2003). The palaeoenvironmental conditions during the P–E boundary interval is evaluated using elemental ratios indicative of detrital input (Ti/Al, Rb/Al and Zr/Al), productivity-related elements and ratios (P_{org} and Ba_{bio}, Ni/Al, Cu/Al and Zn/Al), redox-sensitive elemental proxies (Mn*, V/Cr and V/V + Ni).

4 Results

The range and mean values of major oxides and trace elements of the sediments of the P–E boundary interval in west-central Sinai, Egypt are shown in Table 1. The chemical composition of the DQB differs remarkably from the composition of the underlying and overlying Hanadi and El-Mahmiya members, respectively.

4.1 Major elements

The concentrations of SiO_2, Al_2O_3 and CaO contents that constitute the main sediment components: quartz and/or biogenic silica, phyllosilicates, and carbonates, respectively exhibit abrupt changes across the P–E boundary transition. The sediments of the DQB at W. Feiran, G. Mekattub, and W. Matulla show a wide range of SiO_2 concentrations 8.82–54.84% (mean 26.98%), 8.42–53.76% (mean 30.93%) and 16.8–57.4% (mean 32.26%), respectively. Similarly, the concentration ranges of CaO (3.13–61.71, 6.94–76.83 and 3.82–54.85%) and Al_2O_3 (2.56–20.37, 2.38–17.12 and 4.46–19.35%) in the sediments of the DQB at W. Feiran, G. Mekattub, and W. Matulla, respectively (Table 1). The concentrations of P_2O_5 varied laterally and vertically. Except for the W. Feiran section, the sediments of the DQB yielded the highest average concentrations of P_2O_5; 3.2% for G. Mekattub and 3.06% for W. Matulla. The average concentration of P_2O_5 in the sediments of the DQB at W. Feiran section was 0.84%. A peak of 6.03% and two peaks 5.7 and 5.8% of P_2O_5 concentrations were documented from the DQB at W. Matulla and G. Mekattub sections, respectively. The average concentrations of SiO_2 in the sediments of the Hanadi Member at W. Feiran, G. Mekattub, and W. Matulla are 39.19, 35.58 and 39.5%, respectively, whereas the concentration ranges of SiO_2 in the sediments of the El-Mahmiya Member are 33.56–38.75, 33.74–37.22 and 14.15–21%, respectively. The next most abundant major oxides include Fe_2O_3 (1.46–10.75%), MgO (1.36–4.89%) and P_2O_5 (0.43–6.09%), whereas the concentrations of TiO_2 and MnO are generally low (≤ 1.07%) (Table 1).

Across the P–E transition, concentrations of SiO_2, TiO_2, Al_2O_3 Fe_2O_3, and MgO are notably increased, and in contrast, the concentrations of CaO abruptly decreased. The sediments of W. Feiran, G. Mekattub, and W. Matulla showed abrupt increase of SiO2 across the P–E boundary from 39.03 to 54.84, 31.29 to 53.67 and from 43.06 to 57.4%, respectively. Similarly, they show abrupt increase

Table 1 The ranges and means of elemental concentrations of the Paleocene–Eocene sediments, West Central Sinai, Egypt

	W. Feiran			G. Mekattub			W. Matulla		
	Hanadi	*DQB*	*El-Mahmiya*	*Hanadi*	*DQB*	*El-Mahmiya*	*Hanadi*	*DQB*	*El-Mahmiya*
SiO_2%	39.03–39.35 (39.19)	8.82–54.84 (26.98)	33.56–38.75 (35.42)	31.29–39.87 (35.58)	8.42–53.67 (30.93)	33.74–37.22 (35.5)	32.12–43.35 (39.5)	16.8–57.4 (32.26)	14.15–21 (17.57)
TiO_2%	0.5–0.51 (0.51)	0.11–1.07 (0.47)	0.37–0.49 (0.45)	0.36–0.47 (0.415)	0.1–0.79 (0.39)	0.37–0.47 (0.42)	0.35–0.55 (0.48)	0.23–0.93 (0.46)	0.14–0.24 (0.19)
Al_2O_3%	12.25–12.26 (12.26)	2.56–20.37 (9.05)	11.76–14.08 (12.9)	8.84–11.32 (10.08)	2.38–17.12 (8.63)	11.48–13.43 (12.5)	8.49–12.92 (11.42)	4.46–19.35 (9.56)	2.91–4.64 (3.78)
$^tFe_2O_3$%	4.01–4.04 (4.03)	1.46–4.47 (3.25)	3.96–4.61 (4.35)	3.12–3.89 (3.5)	2.5–10.75 (6.3)	4.27–4.36 (4.32)	2.92–4.89 (3.96)	2.54–6.26 (4.57)	2.61–6.44 (4.53)
MnO%	0.05–0.06 (0.06)	0.01–0.26 (0.012)	0.16–0.19 (0.17)	0.07–0.12 (0.095)	0.02–0.35 (0.13)	0.18–0.19 (0.185)	0.11–0.2 (0.14)	0.02–0.13 (0.08)	0.14–0.16 (0.15)
MgO%	4.22–4.64 (4.43)	1.45–4.38 (2.49)	2.93–3.74 (3.36)	3.07–4.55 (3.81)	1.36–4.89 (2.86)	3.18–3.64 (3.41)	2.91–4.03 (3.62)	1.51–4.55 (2.75)	1.8–2.35 (2.08)
CaO%	26.71–30.36 (28.54)	3.13–61.71 (39.57)	32.33–40.62 (37.21)	33.68–46.82 (40.25)	6.94–76.83 (35.95)	36.52–44.27 (40.4)	28.86–47.44 (35.47)	3.82–54.85 (35.84)	48.12–56.7 (52.4)
Na_2O%	0.15–1.91 (1.03)	6.73–6.37 (6.37)	0.33–2.64 (1.37)	0.47–0.84 (0.66)	0.34–2.9 (1.2)	0.59–0.86 (0.73)	1.02–2.01 (1.51)	0.29–3.66 (1.65)	1.41–6.26 (3.84)
K_2O%	0.44–0.7 (0.57)	0.01–1.65 (0.56)	0.24–0.38 (0.3)	0.2–0.29 (0.25)	0–161 (0.81)	0.35–0.6 (0.48)	0.22–0.75 (0.51)	0.15–1.94 (0.68)	0.53–0.85 (0.69)
P_2O_5%	1.66–1.76 (1.71)	0.76–0.96 (0.84)	0.57–0.82 (0.67)	1.59–1.77 (1.68)	0.62–5.77 (3.2)	0.54–0.75 (0.65)	0.7–1.27 (1.07)	1.05–6.03 (3.06)	0.43–1 (0.72)
LOI%	5.3–7.6 (6.45)	1.7–21.2 (13.43)	2.4–3.7 (3.2)	2.7–2.8 (2.75)	3.2–13.4 (8.52)	0.3–1.8 (1.05)	1–2.3 (1.53)	1.1–22.7 (8.35)	4.8–20.6 (12.7)
V (µg/g)	233–250 (241.5)	135–480 (346.3)	174–222 (203)	185–205 (195)	117–8993 (3014)	214–216 (215)	158–244 (209)	308–7520 (3638)	193–456 (325)
Cr (µg/g)	196–199 (197.5)	49–372 (225.7)	127–130 (128.3)	151–177 (164)	54–2039 (996)	127–129 (128)	127–223 (190)	289–2351 (1402)	204–306 (255)
Ni (µg/g)	263–273 (268)	72–574 (372)	223–322 (257)	230–255 (243)	128–2728 (1581)	271–309 (290)	187–318 (263)	460–1788 (1223)	305–458 (382)
Cu (µg/g)	22–34 (28)	26–108 (67)	15–25 (20)	17–17 (17)	31–350 (175)	34–39 (37)	26–53 (40)	125–344 (245)	86–89 (88)
Zn (µg/g)	247–267 (257)	91–675 (288)	239–310 (276)	237–243 (240)	139–2006 (1034)	307–332 (320)	205–529 (389)	289–1874 (1129)	388–1029 (709)
Rb (µg/g)	16–24 (20)	9–51 (23)	16–18 (17)	15–16 (15.5)	11–58 (31)	23–24 (24)	16–24 (19)	10–69 (27)	19–24 (22)
Sr (µg/g)	1060–1197 (1129)	288–1849 (1132)	1023–1218 (1136)	1350–1419 (1384)	477–1367 (1071)	1142–1238 (1190)	913–1391 (1082)	319–2053 (1442)	1448–1931 (1690)
Y (µg/g)	136–149 (143)	48–86 (62)	41–61 (51)	131–133 (132)	51–174 (133)	47–60 (54)	71–141 (117)	111–139 (127)	31–63 (47)
Zr (µg/g)	123–128 (126)	46–237 (118)	89–102 (95)	100–109 (105)	48–180 (117)	92–103 (98)	95–138 (123)	74–207 (129)	54–82 (68)
Nb (µg/g)	11–11 (11)	4–24 (11.3)	10–14 (13)	8–9 (8.5)	3–16 (40)	11–15 (13)	10–13 (11.67)	3–21 (9)	5–6 (5.5)
Ba (µg/g)	7046–7488 (7267)	2329–24,947 (13901)	4674–4974 (4850)	5589–5694 (5642)	68–3619 (829)	119–3742 (1931)	135–7835 (2702)	153–27,607 (7037)	93–130 (112)

in the concentrations of TiO_2 from 0.5 to 1.07, from 0.36 to 0.79 and from 0.55 to 0.93%, respectively as well as for Al_2O_3 from 12.25 to 20.37, from 8.84 to 17.12 and from 12.86 to 19.35%, respectively. The concentrations of CaO sharply decreased at the P–E transition from 26.71 to 3.13, 46.82 to 6.94 and from 28.86 to 3.82% in the sediments of W. Feiran, G. Mekattub, and W. Matulla sections, respectively (Table 1).

The Si/Al (2.3–4.3) and Ti/Al (0.036–0.058) are relatively homogeneous. The Al-normalized Ti profile shows a slight increase in the sediments of the DQB (Fig. 2). The Ti/Al ratios range between 0.046 and 0.049 for the sediments of the Hanadi Member, between 0.045 and 0.058 for the DQB and between 0.036 and 0.058 for the sediments of El-Mahmiya Member. The Al-normalized Mn, Mg and Ca values show a similar profile with sharp

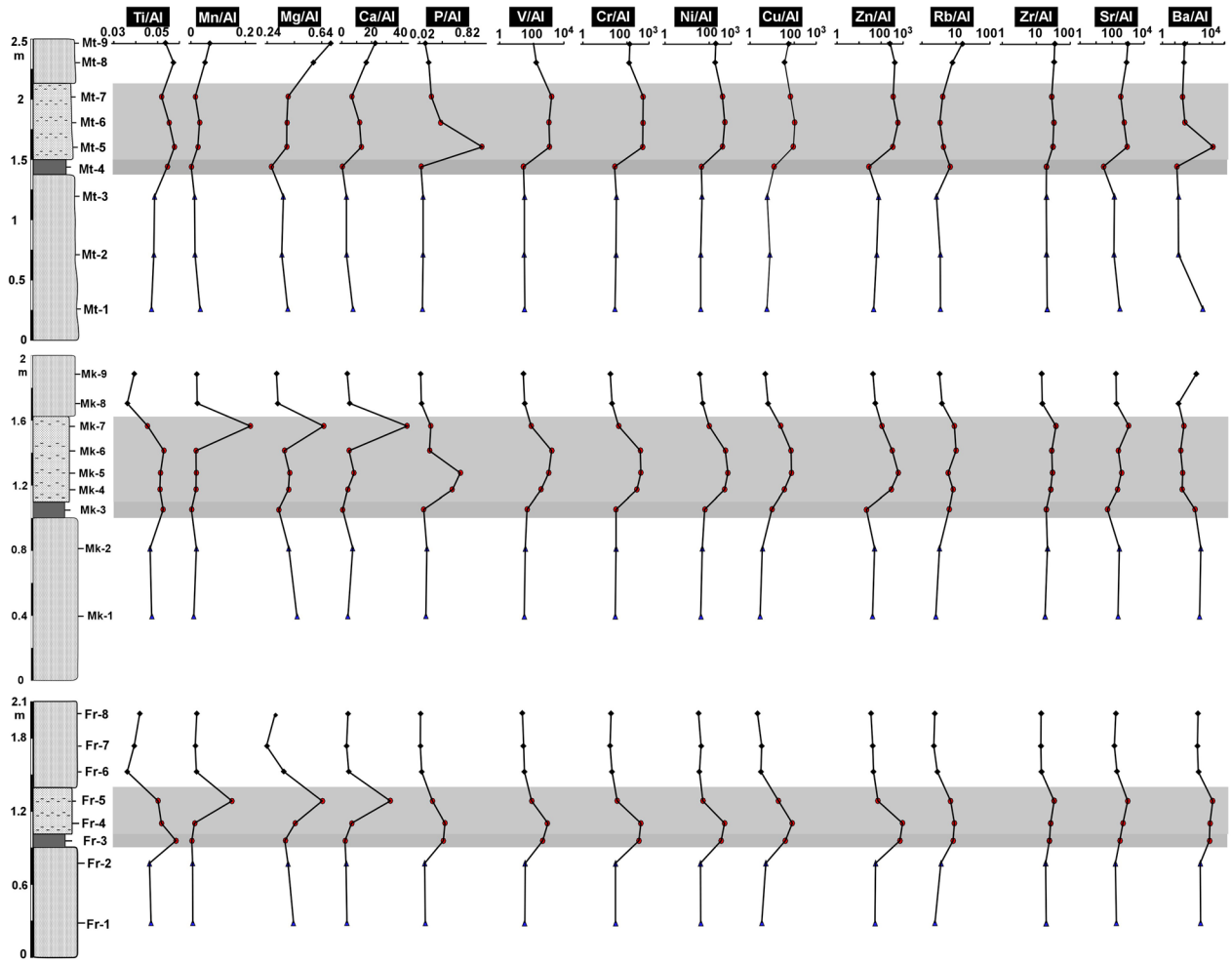

Fig. 2 Vertical profile in the Al-normalized selected major and trace elements in the Paleocene–Eocene sediments, West Central Sinai, Egypt. The grey zone shows the DQB with a dark grey zone demarcates the dark grey shale at the P–E boundary. Note, the positive excursion in the Al-normalized P and Ba values in the lower part of the DQB at W. Matulla section and in the Mn/Al, Ca/Al and Mg/Al values in the upper parts of the DQB at G. Mekattub and W. Feiran sections. The Al-normalized V, Cr, Ni, Cu and Zn display relatively similar vertical trend. The lithostratigraphic units and calcareous nannofossil biozones are shown in Fig. 1

peak in the upper part of the DQB at W. Feiran and G. Mekattub sections. The values of P/Al ratio of the DQB are higher than their counterparts in the sediments of the Hanadi and El-Mahmiya sections. The values of P/Al ratio varied in the sediments of DQB from 0.19 to 1.12, whereas the values P/Al ratio in the sediments of the Hanadi and El-Mahmiya are generally less than 0.2 (Fig. 2).

4.2 Trace elements

Similar to major oxides, the concentrations of trace elements (TE) differed across the P–E boundary; some trace elements (V, Cr, Ni, Cu, Rb, Zr, and Nb) abruptly increased, while others (Zn and Sr) decreased. Trace elements are highly enriched and display wide range of concentrations in the sediments of the DQB comparing to the sediments of the Hanadi and El-Mahmiya members (Table 1). The concentrations of V in the sediments of the DQB fluctuate between 135 and 480 (mean 346 µg/g), 117 and 8993 (mean; 3014 µg/g) and between 308 and 7520 (mean 3683 µg/g) at W. Feiran, G. Mekattub and W. Matulla sections, respectively (Table 1). At W. Feiran, G. Mekattub and W. Matulla sections, the average concentrations of V in sediments of the Hanadi Member are 242, 195 and 209 µg/g, respectively, whereas its average concentrations in the sediments of El-Mahmiya are 203, 215 and 325 µg/g, respectively. An abrupt increase in the concentrations of V (from 250 to 424, 185 to 469 and 244 to 308 µg/g), Cr (from 196 to 256, 151 to 291 and 223 to 289 µg/g), Ni (263 to 470, 230 to 586 and 318 to 460 µg/g) and Cu (34 to 67, 17 to 90

and 41 to 155 μg/g) are documented across the P–E transition at W. Feiran, G. Mekattub and W. Matulla sections, respectively.

The vertical distribution of Al-normalized trace elements (TE) is shown in Fig. (2). The detrital related trace elements (Zr, Rb, and Nb) show a relatively uniform and narrow ranges; Zr/Al ($14–38 \times 10^{-4}$), Nb/Al ($1–4 \times 10^{-4}$) and Rb/Al ($2–16 \times 10^{-4}$). In the studied sections, the Al-normalized ratios of the redox-sensitive elements (V, Cr, Ni, Cu, and Zn) are generally high and variable within the DQB but are generally low and notably uniform in the sediments of the Hanadi and El-Mahmiya members. The ranges of V/Al, Cr/Al, Ni/Al, and Zn/Al in the sediments of the DQB at W. Feiran, G. Mekattub, and W. Matulla sections are $30–1825 \times 10^{-4}$, $28–539 \times 10^{-4}$, $19–700 \times 10^{-4}$ and $22–940 \times 10^{-4}$, respectively (Table 2). In the samples of the Hanadi and El-Mahmiya members, the Al-normalized Cu showed distinct low ratios ($2–8 \times 10^{-4}$). However, relatively high Cu/Al ratios ($36–56 \times 10^{-4}$) were recorded for the samples of El-Mahmiya Member at W. Matulla. The values of the Al-normalized Cu in the sediments of the DQB are high ($35–106 \times 10^{-4}$). The Al-normalized Ba values in the sediments of W. Feiran section are generally higher than that in the other two sections. Their ranges in the sediments of the Hanadi, DQB and El-Mahmiya members at W. Feiran section are $1087–1154 \times 10^{-4}$, $6385–10{,}660 \times 10^{-4}$ and $627–799 \times 10^{-4}$, respectively (Table 2). The values of Ba/Al ratio in the sediments of DQB and El-Mahmiya members at section G. Mekattub are $31–400 \times 10^{-4}$ and 20–526 x 10^{-4}, respectively, whereas their ranges at W. Matulla are $15–11{,}693 \times 10^{-4}$ and $53–60 \times 10^{-4}$, respectively (Table 2).

4.3 Enrichment factors (EF)

The degree of enrichment of the environmentally sensitive major and trace elements (Mn, P, V, Cr, Ni, Cu, Zn and Ba) is determined using enrichment factor (EF; Calvert and Pedersen 1993; Arnaboldi and Meyers 2003; Rimmer 2004; Soliman et al. 2011). It is estimated by normalizing the concentration of the element (X) relative to Al in the sediments and comparing these ratios to the same ratio in average shale. The enrichment factor is determined using the average shale of Li and Schoonmaker (2003) as follows:

$$\mathrm{EF} = \left(\mathrm{X/Al_{sample}/X/Al_{shale}}\right).$$

The major and trace elements of the studied sediments show different levels of enrichment. Of particular note are the wide variation of the EF for V, Cr, Ni, Cu, and Zn.

The sediments of the DQB exhibit a wide range of EF values, but some samples are highly enriched in V, Cr, Ni, Cu and Zn (2–124 fold). At W. Matulla, the ranges of the EF values of V, Cr, Ni, Cu and Zn in the sediments of the DQB are 2–116, 3–53, 8–91, 7–21 and 3–53 (Fig. 3 and Table 3). The enrichment factor values of V, Cr, Ni, Cu and Zn range in the sediments of the DQB at G. Mekattub section from 4 to 124, 3 to 41, 11 to 123, 2 to 15 and 2 to 56, respectively and at W. Feiran section vary from 3 to 15, 2 to 16, 8 to 45, 1 to 10 and 1 to 28, respectively (Fig. 3 and Table 3). The values of the enrichment factor for Mn are slightly low but highly variable varying from 0.05 to 23. The lowest EF values for Mn (0.05, 0.16 and 0.13) were obtained from the dark grey shale layer at the base of the DQB at W. Feiran, G. Mekattub and W. Matulla sections, respectively (Fig. 3).

The enrichment factor values of Ba and P varied remarkably in the studied sections. The highest enrichment factor values of Ba were recorded generally in the sediments of the DQB at W. Feiran (162 and 170) and W. Matulla (177) sections, whereas the sediments of the DQB at G. Mekattub section are highly depleted in Ba ($\mathrm{EF} < 1$). The sediments of the DQB display moderate to high EF values of P at W. Matulla (6–140), G. Mekattub (11–93) and W. Feiran (5–31). Similarly, the EF values for P in the sediments of the Hanadi Member vary from 9 to 10, 16 to 19 and 14 to 15 at W. Matulla, G. Mekattub and W. Feiran sections, respectively, whereas they vary in the sediments of El-Mahmiya Member from 15 to 22, 4 to 7 and 5 to 7, respectively (Table 3).

Generally, the $\mathrm{EF_P}$ values are relatively high in the sediments of the DQB comparing to the underlying and overlying sediments. However, the dark grey shales at the base of the DQB are highly depleted in P (Fig. 3 and Table 3). The $\mathrm{EF_P}$ values are higher at W. Matulla and G. Mekattub sections than at W. Feiran section (Fig. 3). The Ba is highly depleted in the sediments of the P–E boundary. However, a single peak ($\mathrm{EF_{Ba}} = 177$) was recorded from the DQB sediments at W. Matulla section and two successive samples from the DQB at W. Feiran section show $\mathrm{EF_{Ba}}$ of 162 and 170 (Table 3).

4.4 Redox proxies

The redox-sensitive trace elements (e.g. V, Cr, Ni, Cu, and Zn) behave differently under different redox conditions and they are enriched under anoxic (oxygen-free) sediment pore and bottom water conditions. The enrichment of the redox-sensitive trace elements (V, Cr, Ni, Cu, and Zn) and their ratios (V/Cr and V/V + Ni) in marine sediments can be utilized to infer paleoredox conditions (Algeo and Maynard 2004; Tribovillard et al. 2006; Fu et al. 2014). Values of V/Cr ratios < 2 indicate oxic conditions, from 2 to 4.25 indicate dysoxic and > 4.25 show suboxic to anoxic. On the other hand, values of V/(V + Ni) ratio < 0.46 indicate oxic conditions, 0.46–0.60 dysoxic and greater than 0.6 anoxic. The V/Cr ratio is the sediments of the Hanadi

Table 2 The Al-normalized major and trace (multiplied by 10^{-4}) elements of the Paleocene–Eocene sediments, West Central Sinai, Egypt

Sample	Si/Al	Ti/Al	Fe/Al	Mn/Al	Mg/Al	Ca/Al	P/Al	V/Al	Cr/Al	Ni/Al	Cu/Al	Zn/Al	Rb/Al	Sr/Al	Y/Al	Zr/Al	Nb/Al	Ba/Al
Mt-9	4.30	0.05	1.19	0.07	0.71	22.36	0.12	125.61	132.88	198.24	56.21	252.51	15.52	941.62	19.91	34.96	3.30	60
Mt-8	4.00	0.06	1.84	0.05	0.58	16.51	0.18	186.05	124.64	186.84	36.30	419.24	7.89	786.82	25.74	33.56	2.56	53
Mt-7	3.34	0.05	0.66	0.02	0.39	6.74	0.23	1718.90	537.33	408.57	68.17	354.20	4.14	339.62	29.45	28.66	1.44	41
Mt-6	3.38	0.06	1.35	0.03	0.39	12.06	0.39	1162.41	538.79	517.56	105.78	576.34	3.44	587.18	42.80	33.16	1.76	64
Mt-5	3.33	0.06	0.75	0.03	0.38	13.16	1.12	1246.61	514.48	406.56	90.11	339.47	4.39	869.59	54.99	31.38	1.30	11,693
Mt-4	2.62	0.05	0.36	0.00	0.27	0.27	0.04	30.06	28.23	44.90	12.18	28.18	6.77	31.17	10.79	20.23	2.03	15
Mt-3	2.96	0.05	0.50	0.01	0.36	3.03	0.08	35.78	32.77	46.74	6.03	77.71	2.71	138.50	20.72	20.21	1.84	20
Mt-2	2.96	0.05	0.42	0.01	0.35	3.15	0.08	32.88	32.39	41.46	7.80	63.36	3.49	133.52	20.38	19.98	1.86	20
Mt-1	3.34	0.05	0.45	0.03	0.39	7.55	0.07	35.18	28.32	41.63	5.84	45.67	3.51	309.66	15.75	21.06	2.19	1744
Mk-9	2.45	0.04	0.42	0.02	0.31	3.67	0.03	30.36	17.89	38.06	4.80	43.14	3.31	174.18	6.61	14.46	2.05	527
Mk-8	2.60	0.04	0.50	0.02	0.32	5.21	0.05	35.27	21.19	50.90	6.42	54.59	3.86	187.97	9.94	15.15	1.83	20
Mk-7	3.13	0.05	1.39	0.22	0.65	43.66	0.22	93.23	42.56	101.70	25.02	110.30	8.99	1086.94	40.43	38.14	3.70	54
Mk-6	3.27	0.05	0.76	0.02	0.37	4.94	0.19	1824.82	413.75	553.51	71.00	321.19	6.35	250.35	23.97	28.97	1.59	31
Mk-5	3.51	0.05	1.56	0.02	0.40	8.03	0.74	1154.35	421.51	700.03	76.15	601.27	5.94	392.26	48.28	30.28	0.97	42
Mk-4	3.62	0.05	1.77	0.02	0.40	4.10	0.59	385.52	278.90	499.45	35.41	292.57	8.34	227.88	40.91	26.83	1.08	39
Mk-3	2.77	0.05	0.42	0.00	0.33	0.55	0.09	51.82	32.11	64.70	9.98	21.75	6.39	52.62	17.79	19.90	1.79	400
Mk-2	3.12	0.05	0.47	0.02	0.40	7.15	0.15	39.57	32.28	49.08	3.73	50.61	3.32	288.37	28.33	21.42	1.67	1217
Mk-1	3.11	0.05	0.45	0.01	0.46	4.02	0.13	34.29	29.49	42.59	2.85	40.57	2.55	237.02	21.79	18.28	1.54	933
Fr-8	2.33	0.04	0.46	0.02	0.30	4.06	0.04	25.51	19.04	33.14	2.19	35.11	2.38	171.41	6.04	13.89	2.00	720
Fr-7	2.43	0.04	0.43	0.02	0.24	3.10	0.04	29.85	17.07	43.20	3.40	41.53	2.26	137.28	6.86	13.73	1.92	627
Fr-6	2.52	0.04	0.45	0.02	0.36	4.67	0.06	34.17	20.58	35.84	3.14	44.92	2.85	195.84	9.73	14.35	1.68	799
Fr-5	3.05	0.05	0.76	0.15	0.65	32.59	0.25	99.75	36.24	53.04	19.49	71.34	6.94	930.79	38.10	33.78	2.61	10,660
Fr-4	3.54	0.05	2.43	0.01	0.45	6.74	0.46	961.15	418.16	503.12	80.66	939.74	9.02	481.43	28.69	26.81	1.49	6534
Fr-3	3.49	0.06	1.13	0.00	0.37	2.20	0.44	483.92	347.56	351.32	39.43	722.87	8.45	317.63	33.03	24.85	1.02	6385
Fr-2	2.81	0.05	0.43	0.01	0.39	2.94	0.11	38.49	30.21	40.60	5.19	56.64	3.69	163.44	21.02	18.90	1.67	1087
Fr-1	2.83	0.05	0.44	0.01	0.43	3.34	0.12	35.83	30.65	42.07	3.40	53.43	2.42	184.38	22.91	19.69	1.70	1154

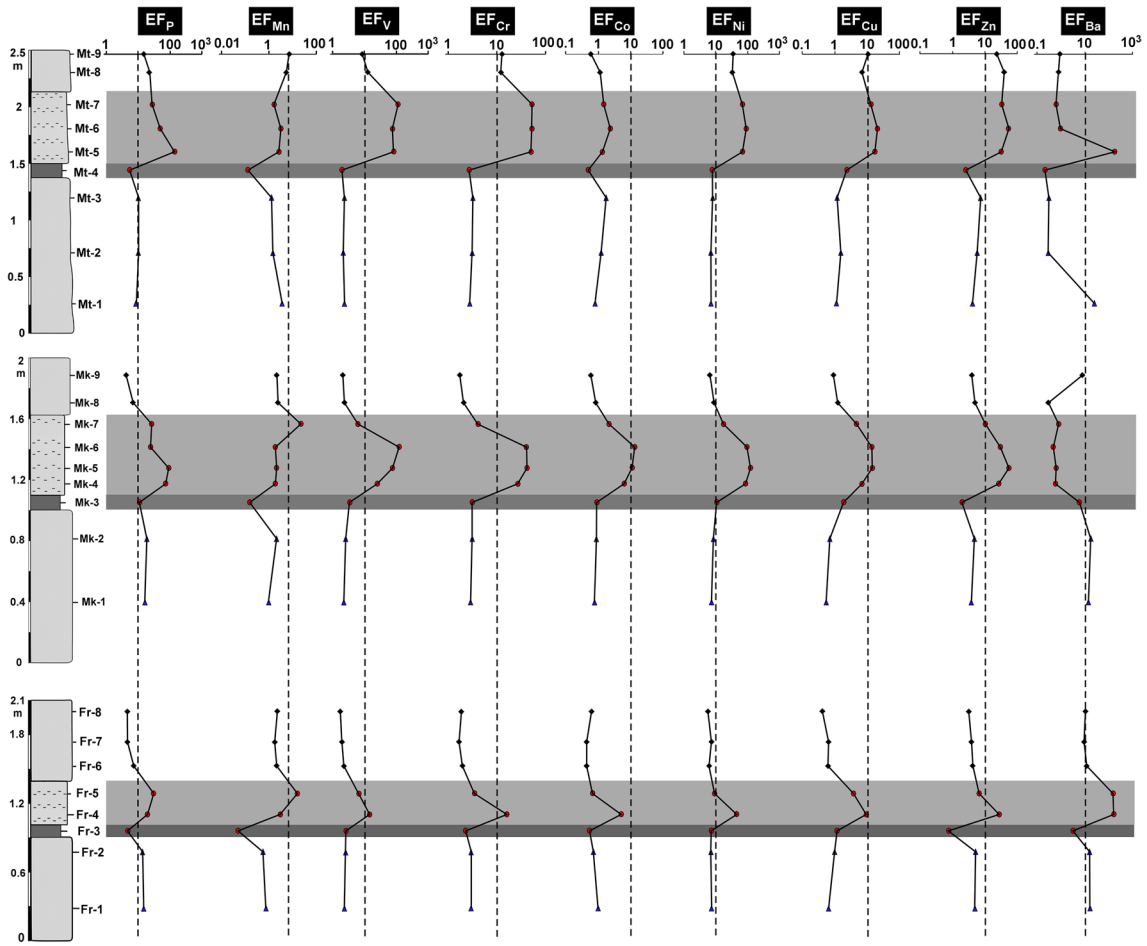

Fig. 3 Vertical profile of the enrichment factor values for some environmentally significant elements in the Paleocene–Eocene sediments, West Central Sinai, Egypt. Note the sediments of the DQB except for the dark grey shales at the base at W. Matulla and G. Mekattub are highly enriched in P, V, Cr, Ni and Zn (EF > 10). The EF values for P and Ba display vertical distribution pattern. The lithostratigraphic units and calcareous nannofossil biozones are shown in Fig. 1

and El-Mahmiya members are generally < 2 and the V/V + Ni ratio are generally ≤ 0.5. The highest values of the V/Cr and V/V + Ni ratios were obtained from the same level in the sediments of the DQB (Table 3, Fig. 4). The V/Cr ratio varies in the sediments of the DQB from 1.29 to 2.76, from 1.38 to 4.41 and from 1.07 to 3.2 at W. Feiran, G. Mekattub and W. Matulla sections, respectively. Similarly, the range of the V/V + Ni ratios in the DQB at W. Feiran, G. Mekattub and W. Matulla sections are 0.46–0.65, 0.44–0.77 and 0.4–0.81, respectively (Table 3).

Another parameter that has been used as redox indicator is the Mn* (Cullers 2002). It is calculated as follows:

$$Mn* = \log\left[\left(Mn_{sample}/Mn_{shale}\right)/Fe_{sample}/Fe_{shale}\right)]$$

The negative values indicate sub-oxic to anoxic bottom conditions, whereas positive Mn* values indicate deposition under oxic and/or nearly suboxic conditions (Cullers 2002). The Mn* value varies in the three sections respectively from 0.81 to 0.93, 1.03 to 1.35 and 1.12 to 1.58. The minimum values (0.16, 0.26 and 0.25) were recorded from the dark grey shale at the base of the Eocene strata (the dissolution interval in the description of Khozyem et al. 2013) (Table 3, Fig. 4). Under low oxygen depositional conditions, Mn is depleted, whereas values close to average shale or slightly above are common deposited under oxic conditions (Brumsack 2006). Relatively low values of Mn/Al indicate sediment pore waters were suboxic for most of the deposition of both successions (Atar et al. 2019). The occasional enrichments of Mn in some samples of the DQB sediments at W. Feiran and G. Mekattub indicate oxic bottom water conditions.

Table 3 The values of enrichment factors of the environmentally related elements, redox-sensitive elemental ratios and parameter and the concentrations of the productivity-related elements

	Enrichment factors								Redox proxies			Productivity proxies	
	EF Mn	EF P	EF V	EF Cr	EF Ni	EF Cu	EF Zn	EF Ba	V/Cr	V/(V + Ni)	Mn*	Porg%	Babio (μg/g)
Mt-9	7.17	15.24	8.49	12.97	34.90	10.94	23.37	0.92	0.95	0.39	1.47	0.17	− 22
Mt-8	5.28	22.31	12.58	12.19	32.85	7.09	38.85	0.80	1.49	0.50	1.14	0.42	− 54
Mt-7	1.72	28.50	116.35	52.54	71.93	13.32	32.82	0.62	3.20	0.81	1.10	0.96	− 150
Mt-6	3.22	48.95	78.68	52.69	91.10	20.69	53.39	0.97	2.16	0.69	1.06	1.24	− 36
Mt-5	2.61	140.20	84.38	50.32	71.56	17.64	31.43	177	2.42	0.75	1.22	2.61	27,430
Mt-4	0.13	5.64	2.04	2.76	7.91	2.39	2.61	0.23	1.07	0.40	0.25	0.38	− 615
Mt-3	1.35	10.24	2.43	3.20	8.22	1.18	7.20	0.31	1.09	0.43	1.12	0.50	− 374
Mt-2	1.46	10.04	2.23	3.16	7.31	1.52	5.87	0.30	1.02	0.44	1.23	0.49	− 378
Mt-1	3.56	8.52	2.38	2.76	7.33	1.13	4.23	27	1.24	0.46	1.58	0.27	7498
Mk-9	2.16	4.19	2.06	1.75	6.71	0.94	4.00	7.99	1.70	0.44	1.40	0.18	3209
Mk-8	2.42	6.78	2.38	2.08	8.95	1.26	5.06	0.30	1.66	0.41	1.37	0.28	− 337
Mk-7	22.46	27.20	6.30	4.20	17.91	4.82	10.24	0.82	2.17	0.48	1.89	0.26	− 26
Mk-6	1.86	24.40	123.52	40.45	97.42	13.89	29.75	0.46	4.41	0.77	1.07	0.92	− 219
Mk-5	2.05	92.85	78.14	41.21	123.18	14.89	55.70	0.63	2.74	0.62	0.80	2.44	− 111
Mk-4	1.89	74.29	26.10	27.28	87.92	6.93	27.11	0.60	1.38	0.44	0.71	2.48	− 152
Mk-3	0.16	11.41	3.50	3.14	11.38	1.94	2.01	6	1.61	0.44	0.26	0.75	2940
Mk-2	2.13	18.63	2.68	3.15	8.65	0.71	4.69	19	1.23	0.45	1.35	0.66	5343
Mk-1	1.00	16.24	2.32	2.89	7.49	0.56	3.76	14	1.16	0.45	1.03	0.73	5140
Fr-8	2.23	4.60	1.73	1.87	5.84	0.43	3.25	11	1.34	0.44	1.37	0.20	4390
Fr-7	1.73	4.61	2.02	1.67	7.60	0.66	3.85	10	1.75	0.41	1.29	0.22	4115
Fr-6	2.10	7.21	2.32	2.01	6.31	0.63	4.15	12	1.66	0.49	1.36	0.31	4507
Fr-5	15.57	30.84	6.75	3.54	9.36	3.76	6.64	162	2.76	0.65	2.00	0.32	14,325
Fr-4	3.03	19.52	14.58	16.33	45.35	9.48	28.07	170	1.29	0.46	0.48	0.92	24,795
Fr-3	0.05	4.89	2.66	2.32	7.67	1.22	0.78	3	1.66	0.47	0.16	1.50	2067
Fr-2	0.58	14.01	2.61	2.96	7.14	1.03	5.24	17	1.28	0.49	0.81	0.67	6560
Fr-1	0.77	14.90	2.43	3.00	7.40	0.66	4.95	18	1.17	0.46	0.93	0.72	7001

4.5 Productivity proxies

A variety of geochemical proxies have been utilized to reconstruct paleoproductivity, among of them, the organically derived phosphorus (P_{org}) and biogenic barium (Ba_{bio}) are the most widely used (Brumsack 2006; Algeo and Ingall 2007; Schoepfer et al. 2015). Inferences concerning paleoproductivity are commonly based on variations in the fluxes rather than absolute/total concentration data (e.g., Algeo et al. 2011; Schoepfer et al. 2015 and references therein). Under conditions favoring their preservation, the fluxes of P_{org}, and Ba_{bio} (or authigenic barite) may serve mutually or individually as proxies for productivity (Paytan and Griffith 2007; Schoepfer et al. 2015). The organic phosphorus fluxes (P_{org}) rather than total phosphorus (P or P_{total}) is estimated as follows:

$$[P_{org}] = [P_{tot}.] - [Al] \times [P/Al]_{det}.$$

The detrital $(P/Al)_{det}$ ratio of 0.0087 is assumed based on the average P and Al concentrations of the upper continental crust (McLennan 2001).

The values of P_{org} varied in the sediments of the DQB from 0.38 to 2.61%, 0.75 to 2.48 and 0.31 to 1.5% at W. Matulla, G. Mekattub and W. Feiran sections, respectively (Table 3). The values of P_{org} in the sediments of the Hanadi and El-Mahmiya vary generally from 0.17 to 0.73% (Table 3, Fig. 4). The high values of EF_P in the sediments of the DQB are consistent with the enrichment of these strata with phosphatic nodules and fish remains (Faris et al. 2015).

On the other hands, the biogenic Ba (Ba_{bio}) that includes all non-detrital Ba was determined as follows:

$$[Ba_{bio}] = [Ba_{tot}] - [Al] \times [Ba/Al]_{det}$$

The $(Ba/Al)_{det}$ ratio of crustal composition that ranges from 0.005 to 0.010 (e.g., Taylor and McLennan 1985) is

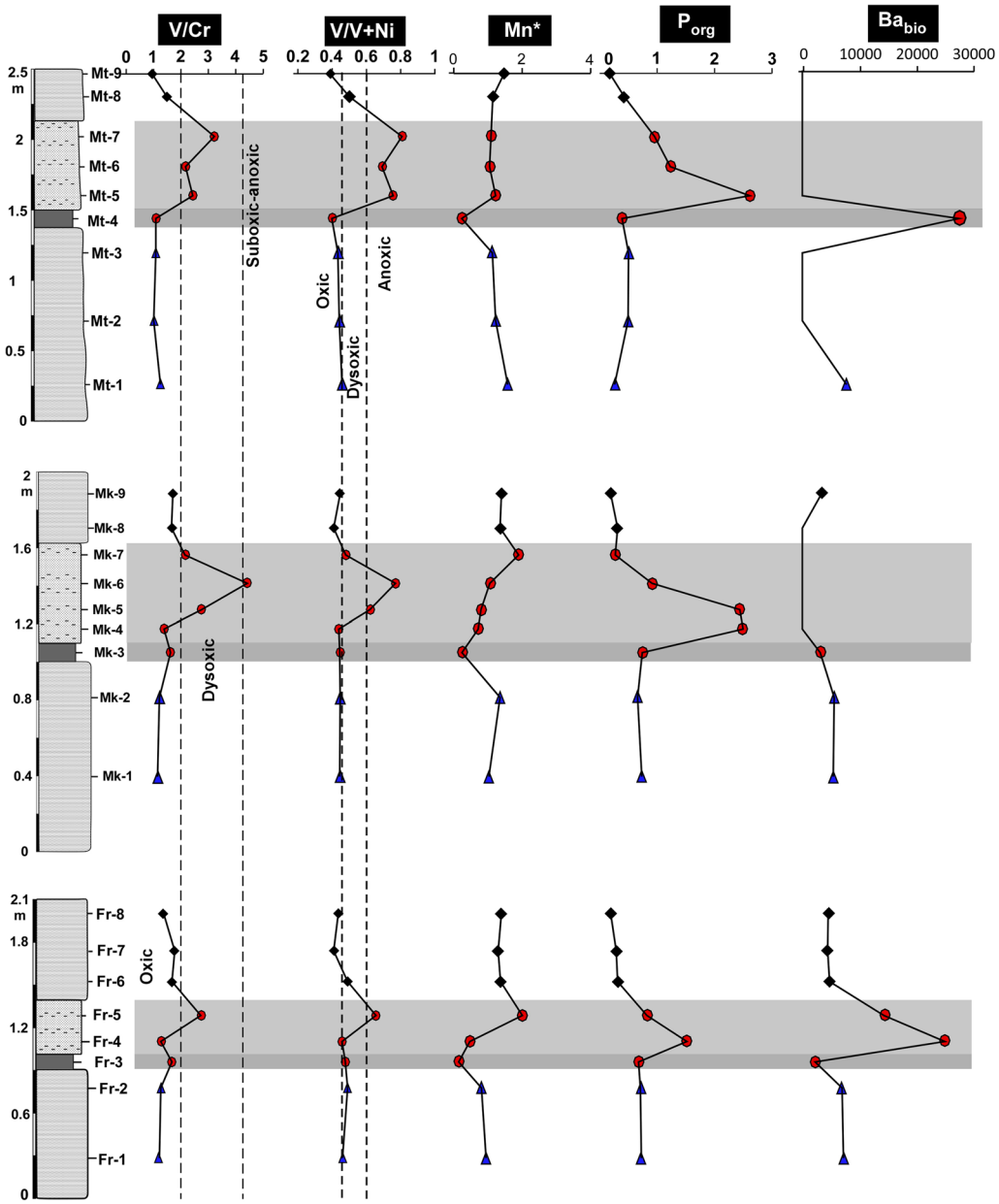

Fig. 4 Vertical variation in the redox proxies (V/Cr, V/V + Ni and Mn*) and the concentrations of productivity proxies (P_{org}. and B_{abio}). The vertical variations in V/Cr and V/V + Ni reveal that the DQB sediments were deposited under dysoxic to anoxic bottom conditions. The positive excursion in the P_{org} immediately above the dark grey shales demarcating the P–E boundary suggests increased primary productivity. The lithostratigraphic units and calcareous nannofossil biozones are shown in Fig. 1

used. Negative Ba_{bio} values may suggest that the Ba in the sediments are generally of detrital origin.

The values of biogenic Ba (Ba_{bio}) are generally high in the sediments of the W. Feiran section. It covers a wide range 4115–24,759 µg/g, whereas the majority of samples from G. Mekattub and W. Matulla sections are represented by non-biogenic Ba (Table 3). The sediments of the Hanadi and the basal part of the DQB display Ba_{bio} concentrations ranging from 2940 to 5434 µg/g and a single peak of Ba_{bio} (27,430 µg/g) was recorded from the DQB at W. Matulla section (Fig. 4). The wide variability of Ba_{bio} content indicates that a considerable part of the Ba_{tot} is composed of biogenic barium (Ba_{bio}), confirming that some intervals experienced high productivity (Table 3).

The Al-normalized Cu, Ni, and Zn, which are strongly related to organic matter, show low values in the sediments of the Hanadi and El-Mahmiya members comparing to the sediments of the DQB (Table 2, Fig. 2). Below the P–E boundary, the average values of Al-normalized Ni, Cu and Zn are 41, 4 and 55 $\times 10^{-4}$ at W. Feiran section, 46, 3 and 46 $\times 10^{-4}$ at G. Mekattub and 43, 7 and 62 $\times 10^{-4}$ at W. Matulla section. Immediately above the P–E boundary, the Ni/Al, Cu/Al, and Zn/Al values varied dramatically among the studied sections. Cu/Al values suddenly increased at the studied section with the highest values recorded from W. Feiran. Across the P–E boundary Ni/Al and Zn/Al increased abruptly at W. Feiran section, Zn/Al suddenly decreased at G. Mekattub and W. Matulla sections associated with no remarkable variations in the Ni/Al value. Above the P–E boundary in the sediments of the DQB all productivity-sensitive elements are highly enriched. At W. Feiran, G. Mekattub and W. Matulla sections, the ranges of Ni/Al (351–503, 499–700 and 407–518 $\times 10^{-4}$, respectively), Cu/Al (39–81, 35–76 and 68–106 $\times 10^{-4}$, respectively) and Zn/Al (723–940, 293–601 and 339–576 $\times 10^{-4}$, respectively) show notable enrichment in the sediments of the DQB. The sediments of the El-Mahmiya Member show a relatively similar Ni/Al, Cu/Al, and Zn/Al values to that of the Hanadi Member at W. Feiran and G. Mekattub sections, whereas the values at W. Matulla section are remarkably higher (Table 2).

5 Discussion

In the present study, the geochemical data of the P–E hemipelagic marine sediments in west-central Sinai is of special interest to interpret the environmental response to the PETM global changes in the southern Tethyan region. The geochemical characterization of the P–E sediments shows that the sediments comprise mainly of admixture of detrital siliciclastic and calcareous biogenous components. In a context of relatively uniform and small variability in the terrigenous related elements, the uniform and relatively limited range of the Al-normalized Si, Ti, Zr, Rb and Nb values suggest that the source rock composition remained unchanged during the P–E boundary interval. The dominantly homogenous fine-grained sediments minimize the effect of hydraulic sorting on sediment composition. Therefore, the elemental enrichment/depletion across the P–E boundary is possibly related to changes in environmental parameters, particularly bioproductivity and bottom redox conditions. The abrupt increase in the concentrations of major oxides (SiO_2, TiO_2, and Al_2O_3) and the coeval depletion in the CaO concentration across the P–E transition are attributed to the $CaCO_3$ dissolution due to increased oceanic acidity (Zachos et al. 2005).

In sediments deposited under such extreme conditions, redox-sensitive trace elements may be strongly enriched (by factors of > 100) in comparison to the average marine shale (März et al. 2008). The Al-normalized redox-sensitive elements (V, Cr, Ni, Cu, and Zn), the ratios (V/Cr and V/V + Ni) and the Mn* values display a relatively similar profile with the absence of significant oscillation throughout the Hanadi and El-Mahmiya members. An interval in the DQB show an extreme elemental enrichment (particularly for V, Ni, Cu and Zn), reflecting a brief period of fully dysoxic to fully anoxic bottom conditions (Algeo and Maynard 2004). Finally, elemental enrichment factors drop to or near the background values within El-Mahmiya Member sediments, suggesting that normal oxygenation like before the PETM was restored. These proxies suggest dominantly oxic to slightly dysoxic bottom conditions. In contrast, these proxies are highly fluctuated in the sediments of the DQB from dysoxic to anoxic and rarely oxic conditions. There is a slight contradiction among these proxies (Figs. 4 and 5). This contradiction is recorded by Khozyem et al. (2013; Fig. 7). The lowest Mn* and EF_{Mn} values were recorded from the dark grey shales at the base of the DQB. The low values are attributed to the removal and diffusion of Mn from sediments to water column under strongly oxygen-depleted bottom waters (Bruland 1983; Cullers 2002; Tribovillard et al. 2006). However, this suggestion contradicts with the corresponding low values of V/Cr and V/V + Ni ratios that show dominantly oxic bottom conditions. The rest of samples show relatively high Mn* values indicating deposition under conditions that are more oxic and this assumption contradicts the dysoxic to anoxic inference by the relatively high values of V/Cr and V/V + Ni ratios. The dark grey shales at the base of the DQB (the condensed clay interval; Khozyem et al. 2013) correspond to a sudden drop in the CaO concentration, possibly correlated with the $CaCO_3$ dissolution interval (Khozyem et al. 2013). The positive correlation between MnO and CaO ($r = 0.8$) suggests that the Mn resides in the carbonate phase, most likely as Mn coatings (Thurow et al. 1992). Therefore, the distribution of Mn in the P–E sediments is primarily controlled by the carbonate content rather than redox conditions. Under oxic–dysoxic conditions, Ni and Cu are deposited mainly in association with the detrital fraction, whereas under anoxic conditions, they are deposited mainly in the form of organometallic complexes. (Tribovillard et al. 2006). Enrichments of redox-sensitive trace elements (V, Cr, Ni, Cu, and Zn) compared to the average shale level within the DQB indicate that pore- and bottom-water was occasionally sub-oxic to anoxic.

Geochemical and micropaleontological data of several sections spanning the PETM in the Peri-Tethys

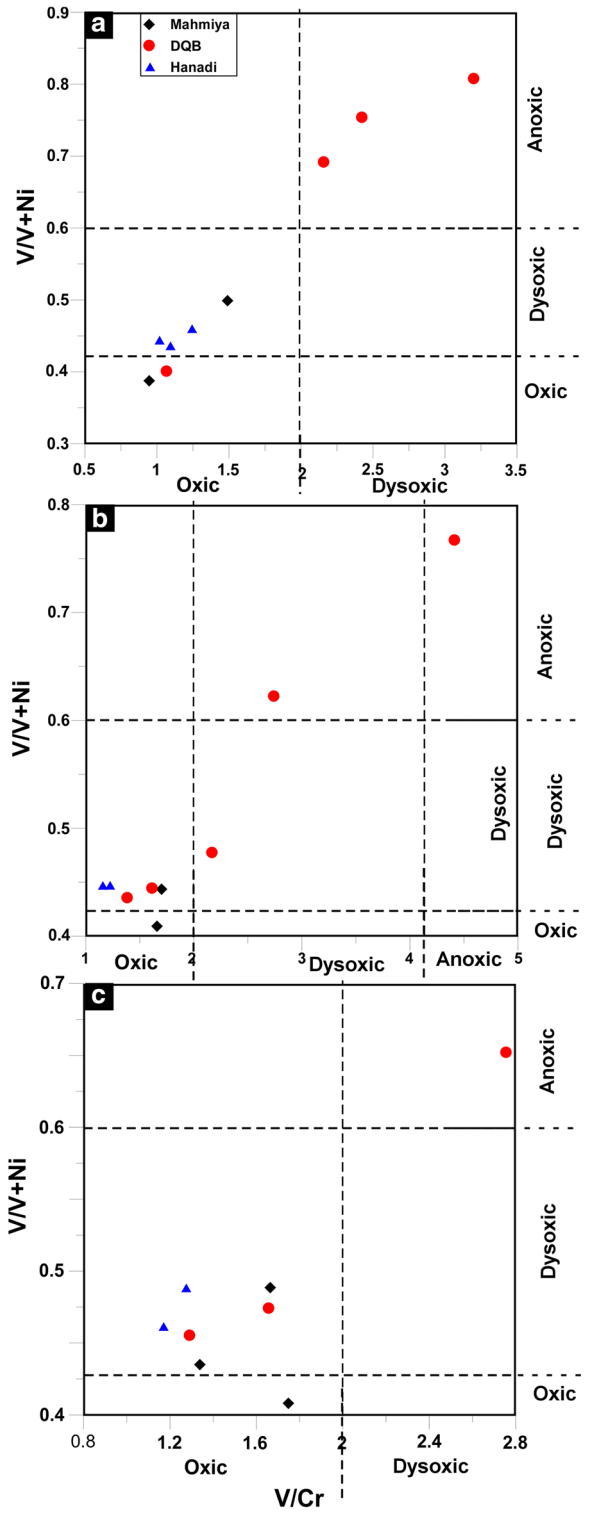

Fig. 5 The relationship between the redox proxies (V/Cr and V/V + Ni) in the Paleocene–Eocene sediments, West Central Sinai, Egypt. **a** W. Matulla, **b** G. Mekattub and **c** W. Feiran sections. Note the sediments of the DQB were deposited under dysoxic to anoxic bottom conditions

regions characterizing anoxic bottom conditions were recognized from Crimea and Uzbekistan (Gavrilova et al. 2018) and Egypt (Speijer et al. 1997; Speijer and Wagner 2002; Soliman 2003; Soliman et al. 2011; Schulte et al. 2011; Khozyem et al. 2013, 2015). A single anoxic event spanning the PETM was recorded at G. Qrieya (Soliman 2003), Dababiya GSSP (Schulte et al. 2011) and W. Nukhul (Khozyem et al. 2013). Khozyem et al. (2015) recognized two anoxic events demarcated by negative Ce-anomalies at Dababiya GSSP and associated with enrichment of redox-sensitive elements and the formation of idiomorphic and framboidal pyrite. The development of bottom anoxicity during the PETM was attributed to: (1) the inflow of poorly oxygenated intermediate water into the epicontinental circulation combined with enhanced upwelling and increased primary productivity (Speijer and Wagner 2002), (2) water-column salinity/temperature stratification and eutrophication (Schulte et al. 2011; Khozyem et al. 2015) and (3) increased ocean acidification due to methane hydrate release (Khozyem et al. 2015). Water column stratification prevented light penetration and water ventilation and increased surface water productivity and organic matter influx to the seafloor, which in turn led to consumption of bottom oxygen by bacteria (Schulte et al. 2011; Khozyem et al. 2015). Fluctuations between anoxic and suboxic or dysoxic bottom waters were inferred by trace fossils (Faris et al. 2015) and by the benthic foraminiferal records in the DQB sediments (Speijer and Wagner 2002).

The contents and the vertical trends of P_{org} and Ba_{bio} across the P–E boundary vary among the studied sections and show inconsistent relationship suggesting a local influence on the behaviour of the two elements. The occasional high positive excursion of Ba_{bio} (up to 2.7%) in the sediments of the DQB at W. Feiran and W. Matulla sections compared with the concentration in average shale (0.058%) possibly indicate increased organic productivity during the earliest Eocene in west-central Sinai. This scenario is supported by increased nutrient supply through coeval enrichment of P_{org} (up to 2.6%). The relatively high P_{org} content in the basal sediments of the DQB coincides with the low Mn* value suggesting that bottom condition was not anoxic (Fig. 4). Phosphate (P) is generally depleted under anoxic condition because it is easily remobilized from the sediments and diffuses back to water column. The negative correlation with detrital-related elements (Ti and Zr) suggests that the coeval enrichment of the Ni, Cu, and Zn in the sediments of the DQB further supports enhanced primary productivity during earliest Eocene through the formation of organometallic complexation with organic matter and/or the removal of surface waters by plankton growth.

Several micropaleontological and geochemical proxies at several oceanic sites support the idea of increased upwelling and fluxes of nutrients enhanced primary productivity during the PETM (Schmitz et al. 1997a, b; Bains et al. 2000; Crouch et al. 2003). The abundance of tiny biogenic barite crystals (up to tens of microns) and opal-CT within the P–E boundary sediments at W. Matulla and Abu-Zenima suggests enhanced primary productivity (Bolle et al. 2000). At the Dababiya (GSSP), the occurrence of pyrite, barite, phosphate concretions, high TOC combined with enrichment of the productivity-related elements (P, Zn, and V) in the sediments of the PETM suggest increased primary productivity (Soliman et al. 2011; Khozyem et al. 2015). Enhanced productivity was attributed to an increase in the input of detrital minerals and organic matter (i.e., fossilized wood; Dupuis et al. 2003) to the shallow zones of the southern Tethyan margin basin. The complex mixture of clay minerals recorded at the Dababiya (Bolle et al. 2000; Schulte et al. 2011; Soliman et al. 2011; Khozyem et al. 2015) suggests that intensive chemical weathering and erosion of sources on the continent by the late Paleocene-Early Eocene sea-level and climate changes (Dupuis et al. 2003). The Early Eocene climate models suggested that the Tethyan southern margin has been affected by intermittent upwelling episodes initiated by increased atmospheric contrast between the arid, sub-tropical coastal zone and the humid, tropical continent intensifying the off-shore directed Ekman transportation (Speijer and Wagner 2002). The presence of condensed phosphate in the middle part of the DQB is consistent with upwelling activity (Bolle et al. 2000).

Bottom-water redox condition exerts a strong influence on the accumulation of productivity-sensitive elements and there is interplay between productivity and bottom redox conditions (Tribovillard et al. 2006). Under reducing conditions, the burial fluxes of P_{org} and Ba_{bio} are diminished owing to the reductive dissolution of Mn–Fe-oxyhydroxide particles, thus releasing adsorbed P, and barite crystals, releasing Ba (Tyson 2005), whereas oxidizing conditions facilitate the preservation of P_{org} and Ba_{bio} within the sediments. At G. Mekattub (sample Mk-5), a coeval positive excursion in P_{org}, EF_P, V/Cr, and V/V + Ni. Similarly, at W. Matulla section, sample Mt-5 displays high values of EF_P and EF_{Ba}, P_{org} and Ba_{bio} content corresponding to relatively high values of V/Cr and V/V + Ni. The dysoxic to slightly anoxic bottom conditions were not severe enough to fully release the P and Ba from sediments. Some of the released P and Ba are possibly retained in the sediment and ultimately incorporated into authigenic P- and Ba-bearing mineral phases. High P accumulation rates during the Cenomanian–Turonian oceanic anoxic event (OAE2) was associated with high organic influx suggesting that P accumulation is a good indicator for productivity changes unless the bottom conditions change to severely anoxic (Mort et al. 2007).

6 Conclusions

Geochemical analysis of the Esna Shale sediments at three well-dated stratigraphic sections in the west-central Sinai, Egypt enabled interpreting environmental changes across the Paleocene–Eocene transition. Samples were collected from the uppermost Eocene Hanadi Member and the lowermost Eocene Dababiya Quarry Bed (DQB) El-Mahmiya members. Geochemical proxy investigation of the P–E boundary interval revealed the following conclusions:

1. The concentrations of major (SiO_2, TiO_2, Al_2O_3 Fe_2O_3, MgO) and trace (V, Cr, Ni, Cu, Rb, and Zr) elements display remarkable positive excursion, whereas the concentrations of CaO, MnO, Sr, and Zn show abrupt negative excursion.
2. The Al-normalized environmental-sensitive elements (Mn, P, V, Cr, Ni, Cu, Zn, and Ba) exhibit a relatively uniform trend in the sediments of the Hanadi and El-Mahmiya members. On the other hand, they are highly enriched in the sediments of the DQB.
3. At the very base of the PETM event beds (transition from Hanadi to DQB), the dark grey shale is virtually depleted in CaO suggesting a brief period of carbonate dissolution, possibly associated with global ocean acidification.
4. The enrichment of the redox-sensitive trace elements and the their ratios (V/Cr and V/V + Ni) within the sediments of the P–E boundary interval suggest normal oxygenated conditions during deposition of the El-Hanadi Member followed by a gradual onset of oxygen depletion during the deposition of DQB. The sediments of the DQB show high overall V/(V + Ni) values and data plot within the suboxic and rarely anoxic fields, whereas the Hanadi and El-Mahmiya samples consistently show lower values than do the DQB. Similarly, V/Cr values show similar differences, and values are weighted towards suboxic to anoxic conditions for the DQB and towards oxic conditions for the Hanadi and El-Mahmiya.
5. A significant enrichment in P_{org} and Ba_{bio} contents in the sediments of the DQB indicates increased primary productivity induced by increasing nutrients supply through terrestrial runoff and enhanced upwelling process.
6. The enrichment in productivity-related elements in line with enriched redox-sensitive elements suggests that the reducing bottom conditions were not severe enough to fully release and diffuse back the P and Ba from sediments to seawaters.

Acknowledgements
This project was funded by the Deanship of Scientific Research (DSR), King Abdulaziz University, Jeddah, under Grant No. (D-112-150-1441). The authors, therefore, gratefully acknowledge DSR technical and financial support. The authors are very grateful for the editor and reviewers for their constructive comments and editorial handling.

Authors' contributions
The author read and approved the final manuscript.

Funding
This work was funded by the Deanship of Scientific Research (DSR), King Abdulaziz University, Jeddah, under Grant No. (D-112-150-1441).

Availability of data and materials
The datasets used in the current study are available from the corresponding author on reasonable request.

Competing interests
The author declares that there is no competing interests.

Author details
[1] Marine Geology Department, Faculty of Marine Science, King Abdulaziz University, P.O. Box 80200, Jeddah 21589, Saudi Arabia. [2] Geology Department, Faculty of Science, Tanta University, Tanta 31527, Egypt.

Received: 12 December 2019 Accepted: 7 March 2020
Published online: 20 March 2020

References

Abu Shama, A., Faris, M., & Al-Wosabi K. A. (2007). Upper Paleocene–lower Eocene calcareous nannofossil biostratigraphy and Paleoecology of Gebel Matulla section, Southwestern Sinai, Egypt. In *Proceedings of the 5th international conference on the Geology of Africa*, (pp. 33–51), Assiut.

Alegret, L., Ortiz, S., Orue-Etxebarria, X., Bernaola, G., Baceta, J. I., Monechi, S., et al. (2009). The Paleocene–Eocene thermal maximum: new data on microfossil turnover at the Zumaia section, Spain. *Palaios, 24,* 318–328.

Algeo, T. J., & Ingall, E. (2007). Sedimentary Corg: P ratios, Paleocean ventilation, and Phanerozoic atmospheric pO2. *Palaeogeography, Palaeoclimatology, Palaeoecology, 256,* 130–155.

Algeo, T. J., Kuwahara, K., Sano, H., et al. (2011). Spatial variation in sediment fluxes, redox conditions, and productivity in the Permian-Triassic Panthalassic Ocean. *Palaeogeography, Palaeoclimatology, Palaeoecology, 308,* 65–83.

Algeo, T. J., & Maynard, J. B. (2004). Trace-element behavior and redox facies in core shales of Upper Pennsylvanian Kansas-type cyclothems. *Chemical Geology, 206,* 289–318.

Almogi-Labin, A., Beim, A., & Sass, E. (1993). Late Cretaceous upwelling system along the southern Tethys margin (Israel): interrelationship between productivity, bottom water environments and organic matter preservation. *Paleoceanography, 8,* 671–690.

Arnaboldi, M., & Meyers, P. A. (2003). Geochemical evidence for paleoclimatic variations during deposition of two late Pliocene sapropels from the Vrica section, Calabria. In P. A. Meyers & A. Negri (Eds.), *Paleoclimatic and Paleoceanographic records in Mediterranean Sapropels and Mesozoic Black Shales*. *Palaeogeography, Palaeoclimatology, Palaeoecology* (Vol. 190, pp. 257–271).

Atar, E., März, C., Schnetger, B., et al. (2019). Local to global controls on the deposition of organic-rich muds across the Late Jurassic Laurasian Seaway. *Journal of the Geological Society*. https://doi.org/10.1144/jgs2019-031.

Aubry, M.-P., Ouda, Kh, Dupuis, C., et al. (2007). Global Standard Stratotype—Section and Point (GSSP) for the base of the Eocene Series in the Dababiya Section (Egypt). *Episodes, 30,* 271–286.

Bains, S., Norris, R. D., Corfield, R. M., & Faul, K. L. (2000). Termination of global warmth at the Palaeocene/Eocene boundary through productivity feedback. *Nature, 407,* 171–174.

Bolle, M.-P., & Adatte, T. (2001). Palaeocene early Eocene climatic evolution in the Tethyan realm: clay mineral evidence. *Clay Minerals, 36,* 249–261.

Bolle, M.-P., Tantawy, A. A., Pardo, A., et al. (2000). Climatic and environmental changes documented in the upper Paleocene to lower Eocene of Egypt. *Eclogae Geologicae Helvetiae, 93,* 33–51.

Bowen, G. J., Clyde, W. C., Koch, P. L., et al. (2002). Mammalian dispersal at the Paleocene/Eocene boundary. *Science, 295,* 2062–2065.

Bruland, K. W. (1983). Trace elements in sea-water. In J. P. Riley & R. Chester (Eds.), *Chemical oceanography* (Vol. 8, pp. 157–220). London: Academic Press.

Brumsack, H.-J. (2006). The trace metal content of recent organic carbon-rich sediments: implications for Cretaceous black shale formation. *Palaeogeography, Palaeoclimatology, Palaeoecology, 232,* 344–361.

Calvert, S. E., & Pedersen, T. F. (1993). Geochemistry of recent oxic and anoxic marine sediments: implications for the geological record. *Marine Geology, 113,* 67–88.

Cao, W., Xi, D., Melinte-Dobrinescu, M. C., et al. (2018). Calcareous nannofossil changes linked to climate deterioration during the Paleocene–Eocene thermal maximum in Tarim Basin, NW China. *Geoscience Frontiers, 9,* 1465–1478.

Crouch, E. M., Dickens, G. R., Brinkhuis, H., et al. (2003). The Apectodinium acme and terrestrial discharge during the Paleocene–Eocene thermal maximum: new palynological, geochemical and calcareous nannoplankton observations at Tawanui, New Zealand. *Palaeogeography, Palaeoclimatology, Palaeoecology, 194,* 387–403.

Cullers, R. L. (2002). Implications of elemental concentrations for provenance, redox conditions, and metamorphic studies of shales and limestones near Pueblo, CO, USA. *Chemical Geology, 191,* 305–327.

Dupuis, C., Aubry, M. P., Steurbat, E., et al. (2003). The Dababiya Quarry section: lithostratigraphy, clay mineralogy, geochemistry and paleontology. *Micropaleontology, 49,* 41–59.

Faris, M., Ghandour, I. M., Zahran, E., et al. (2015). Calcareous nannoplankton changes during the Palaeocene–Eocene thermal maximum in West Central Sinai, Egypt. *Turkish Journal of Earth Sciences, 24,* 475–493.

Fu, X., Wang, J., Chen, W., et al. (2014). Elemental geochemistry of the early Jurassic black shales in the Qiangtang Basin, eastern Tethys: constraints for palaeoenvironment conditions. *Geological Journal, 51,* 443–454.

Gavrilova, Y. O., Golovanovaa, O. V., Shchepetovaa, E. V., & Pokrovskya, B. G. (2018). Lithological and Geochemical Characteristics of the Paleocene/Eocene Sediments corresponding to the PETM Biospheric Event in the Eastern Crimea (Nasypnoe Section). *Lithology and Mineral Resources, 53,* 337–348.

Gawenda, P., Winkler, W., Schmitz, B., et al. (1999). Climate and bioproductivity control on carbonate turbidite sedimentation (Paleocene to earliest Eocene, Gulf of Biscay, Zumaia, Spain). *Journal of Sedimentary Research, 69*(6), 1253–1261.

Keller, G., Mateo, P., Punekar, J., et al. (2018). Environmental changes during the Cretaceous-Paleogene mass extinction and Paleocene–Eocene thermal maximum: implications for the Anthropocene. *Gondwana Research, 56,* 69–89.

Kender, S., Stephenson, M. H., Riding, J. B., et al. (2012). Marine and terrestrial environmental changes in NW Europe preceding carbon release at the Paleocene–Eocene transition. *Earth and Planetary Science Letters, 353–354,* 108–120.

Kennett, J. P., & Stott, L. D. (1991). Abrupt deep-sea warming, palaeoceanographic changes and benthic extinctions at the end of the Paleocene. *Nature, 353,* 225–229.

Khozyem, H., Adatte, T., Spangenberg, J. E., et al. (2013). Palaeoenvironmental and climatic changes during the Paleocene–Eocene thermal maximum (PETM) at the Wadi Nukhul Section, Sinai, Egypt. *Journal of the Geological Society, 170,* 341–352.

Khozyem, H., Adatte, T., Spangenberg, J. E., et al. (2015). New geochemical constraints on the Paleocene–Eocene thermal maximum: Dababiya GSSP, Egypt. *Palaeogeography, Palaeoclimatology, Palaeoecology, 429,* 117–135.

Li, Y. H., & Schoonmaker, J. E. (2003). Chemical composition and mineralogy of marine sediments. In H. D. Holland & K. K. Turekian (Eds.), *Treatise on Geochemistry* (pp. 3469–3503). Amsterdam: Elsevier Ltd.

März, C., Poulton, S. W., Beckmann, B., et al. (2008). Redox sensitivity of P cycling during marine black shale formation: dynamics of sulfidic and anoxic, non-sulfidic bottom waters. *Geochimica et Cosmochimica Acta, 72,* 3703–3717.

McInerney, F. A., & Wing, S. L. (2011). The Paleocene–Eocene thermal maximum: a perturbation of carbon cycle, climate, and biosphere with implications for the future. *Annual Review of Earth and Planetary Sciences, 39,* 489–516.

McLennan, S. M. (2001). Relationships between the trace element composition of sedimentary rocks and upper continental crust. *Geochemistry, Geophysics, Geosystems, 2,* 1021.

Mort, H. P., Adatte, T., Föllmi, K. B., et al. (2007). Phosphorus and the roles of productivity and nutrient recycling during oceanic anoxic event 2. *Geology, 35,* 483–486.

Murphy, B. H., Farley, K. A., & Zachos, J. C. (2010). An extraterrestrial ^{3}He-based timescale for the Paleocene–Eocene thermal maximum (PETM) from Walvis Ridge, IODP Site 1266. *Geochimica et Cosmochimica Acta, 74,* 5098–5108.

Obaidalla, N. A., Abdel-Maksoud, N. A., Hosny, A. M., et al. (2017). Nature of the Paleocene/Eocene (P/E) boundary in Sinai, Egypt. *Journal of African Earth Sciences, 136,* 44–60.

Pälike, C., Delaney, M. L., & Zachos, J. C. (2014). Deep-sea redox across the Paleocene–Eocene thermal maximum. *Geochemistry, Geophysics, Geosystems, 15,* 1038–1053.

Paytan, A., & Griffith, E. M. (2007). Marine barite: recorder of variations in ocean export productivity. *Deep Sea Research Part II: Topical Studies in Oceanography, 54,* 687–705.

Rimmer, S. M. (2004). Geochemical paleoredox indicators in Devonian-Mississippian black shales, Central Appalachian Basin (USA). *Chemical Geology, 206,* 373–391.

Riquier, L., Tribovillard, N., Averbuch, O., et al. (2006). The Late Frasnian Kellwasser horizons of the Harz Mountains (Germany): two oxygendeficient periods resulting from contrasting mechanisms. *Chemical Geology, 233,* 137–155.

Röhl, U., Westerhold, T., Bralower, T. J., et al. (2007). On the duration of the Paleocene–Eocene thermal maximum (PETM). *Geochemistry, Geophysics, Geosystems, G3,* Q12002.

Schmitz, B., Asaro, F., Molina, E., et al. (1997a). High-resolution iridium, $\delta^{13}C$, $\delta^{18}O$, foraminifera and nannofossil profiles across the latest Paleocene benthic extinction event at Zumaya, Spain. *Palaeogeography, Palaeoclimatology, Palaeoecology, 133,* 49–68.

Schmitz, B., Charisi, S. D., Thompson, E. I., et al. (1997b). Barium, SiO_2-excess and P_2O_5 as proxies of biological productivity in the Middle East during the Paleocene and the latest Paleocene benthic extinction event. *Terra Nova, 9,* 95–99.

Schoepfer, S. D., Shen, J., Wei, H., et al. (2015). Total organic carbon, organic phosphorus, and biogenic barium fluxes as proxies for paleomarine productivity. *Earth Science Reviews, 149,* 23–52.

Schoon, P. L., Heilmann-Clausen, C., Pagh Schultz, B., et al. (2015). Warming and environmental changes in the eastern North Sea Basin during the Palaeocene–Eocene thermal maximum as revealed by biomarker lipids. *Organic Geochemistry, 78,* 79–88.

Schulte, P., Scheibner, C., & Speijer, R. P. (2011). Fluvial discharge and sea-level changes controlling black shale deposition during the Paleocene–Eocene thermal maximum in the Dababiya Quarry section, Egypt. *Chemical Geology, 285,* 167–183.

Self-Trail, J. M., Powars, D. S., Watkins, D. K., et al. (2012). Calcareous nannofossil assemblage changes across the Paleocene–Eocene thermal maximum: evidence from a shelf setting. *Marine Micropaleontology, 92–93,* 61–80.

Sluijs, A., Bowen, G., Brinkhuis, H., et al. (2007). The Palaeocene-Eocene Thermal Maximum super greenhouse: biotic and geochemical signatures, age models and mechanisms of global change. In M. Williams, A. M. Haywood, F. J. Gregory, et al. (Eds.), *Deep-time perspectives on climate change: marrying the signal from computer models and biological proxies* (pp. 323–349). Micropalaeontological Society, Geological Society London, Special Publication.

Sluijs, A., Schouten, S., Pagani, M., et al. (2006). Subtropical Arctic Ocean temperatures during the Palaeocene/Eocene thermal maximum. *Nature, 441,* 610–613.

Soliman, M. F. (2003). Chemostratigraphy of the Paleocene/Eocene (P/E) boundary sediments at Gabal el-Qreiya, Nile Valley, Egypt. *Micropaleontology*, *49*(Suppl_1), 123–138. https://doi.org/10.2113/49.Suppl_1.123.

Soliman, M. F., Aubry, M.-P., Schmitz, B., & Sherrell, R. M. (2011). Enhanced coastal paleoproductivity and nutrient supply in Upper Egypt during the Paleocene/Eocene thermal maximum (PETM): mineralogical and geochemical evidence. *Palaeogeography, Palaeoclimatology, Palaeoecology, 310,* 365–377.

Soua, M., Zaghbib-Turki, D., Ben Jemia, H., et al. (2011). Geochemical Record of the Cenomanian-Turonian Anoxic Event in Tunisia: is it Correlative and Isochronous to the Biotic Signal? *Acta Geologica Sinica, 85*(5), 801–840.

Speijer, R. P., Schmitz, B., & Van Der Zwann, G. J. (1997). Benthic foraminiferal extinction and repopulation in response to latest Paleocene Tethyan anoxia. *Geology*, *25*, 683–686.

Speijer, R. P., & Wagner, T. (2002). Sea-level changes and black shales associated with the late Paleocene thermal maximum: organic-geochemical and micropaleontologic evidence from the southern Tethyan margin (Egypt-Israel). *Geological Society of America Special Paper, 356,* 533–549.

Stassen, P., Dupuis, C., Steurbaut, E., et al. (2012). Perturbation of a Tethyan coastal environment during the Paleocene–Eocene thermal maximum in Tunisia (Sidi Nasseur and Wadi Mezaz). *Palaeogeography, Palaeoclimatology, Palaeoecology, 317–318,* 66–92.

Tawfik, H. A., Ghandour, I. M., Maejima, W., Armstrong-Altrin, J. S., & Abdel-Hameed, A. T. (2017). Petrography and geochemistry of the siliciclastic Araba Formation (Cambrian), east Sinai, Egypt: implications for provenance, tectonic setting and source weathering. *Geological Magazine, 154,* 1–23.

Taylor, S. R., & McLennan, S. M. (1985). *The continental crust: its composition and evolution*. Geoscience Texts: Blackwell Scientific Publications.

Thurow, J., Brumsack, H.-J., Rullkötter, J., et al. (1992). The Cenomanian/Turonian boundary event in the Indian Ocean—A key to understand the global picture. In R. A. Duncan, D. K. Rea, R. B. Kidd, et al. (Eds.), *Synthesis of results from scientific drilling in the Indian Ocean* (Vol. 70, pp. 253–273). American Geophysical Union, Geophysical Monograph.

Tribovillard, N., Algeo, T. J., Lyons, T., & Riboulleau, A. (2006). Trace metals as paleoredox and paleoproductivity proxies: an update. *Chemical Geology, 232,* 12–32.

Tyson, R. V. (2005). The "productivity versus preservation" controversy; cause, flaws, and resolution. In: N. B. Harris (Ed.), Deposition of organic-carbon-rich sediments: models, mechanisms, and consequences. *Society for Sedimentary Geology (SEPMSSG) Special Publication* (Vol. 82, pp. 17–33).

Westerhold, T., Röhl, U., Donner, B., et al. (2011). A complete highresolution Paleocene benthic stable isotope record for the central Pacific (ODP Site 1209). *Paleoceanography, 26,* PA2216.

Zachos, J. C., Dickens, G. R., & Zeebe, R. E. (2008). An early Cenozoic perspective on greenhouse warming and carbon-cycle dynamics. *Nature, 451,* 279–283.

Zachos, J. C., Röhl, U., Schellenberg, S. A., et al. (2005). Rapid acidification of the ocean during the Paleocene-Eocene Thermal Maximum. *Science*, *308*, 1611–1615.

Zachos, J. C., Schouten, S., Bohaty, S., et al. (2006). Extreme warming of mid-latitude coastal ocean during the Paleocene–Eocene thermal maximum: inferences from TEX86 and isotope data. *Geology, 34,* 737–740.

Publisher's Note